Cooperative subunit dynamics modulate p97 function

Rui Huang[a,b,c,d,1], Zev A. Ripstein[a,b], John L. Rubinstein[a,b,e], and Lewis E. Kay[a,b,c,d,1]

[a]Program in Molecular Medicine, The Hospital for Sick Children, Toronto, ON M5G 1X8, Canada; [b]Department of Biochemistry, University of Toronto, Toronto, ON M5S 1A8, Canada; [c]Department of Molecular Genetics, University of Toronto, Toronto, ON M5S 1A8, Canada; [d]Department of Chemistry, University of Toronto, Toronto, ON M5S 3H6, Canada; and [e]Department of Medical Biophysics, University of Toronto, Toronto, ON M5G 1L7, Canada

Edited by Peter E. Wright, The Scripps Research Institute, La Jolla, CA, and approved November 20, 2018 (received for review September 7, 2018)

p97 is an essential hexameric AAA+ ATPase involved in a wide range of cellular processes. Mutations in the enzyme are implicated in the etiology of an autosomal dominant neurological disease in which patients are heterozygous with respect to p97 alleles, containing one copy each of WT and disease-causing mutant genes, so that, in vivo, p97 molecules can be heterogeneous in subunit composition. Studies of p97 have, however, focused on homohexameric constructs, where protomers are either entirely WT or contain a disease-causing mutation, showing that for WT p97, the N-terminal domain (NTD) of each subunit can exist in either a down (ADP) or up (ATP) conformation. NMR studies establish that, in the ADP-bound state, the up/down NTD equilibrium shifts progressively toward the up conformation as a function of disease mutant severity. To understand NTD functional dynamics in biologically relevant p97 heterohexamers comprising both WT and disease-causing mutant subunits, we performed a methyl-transverse relaxation optimized spectroscopy (TROSY) NMR study on a series of constructs in which only one of the protomer types is NMR-labeled. Our results show positive cooperativity of NTD up/down equilibria between neighboring protomers, allowing us to define interprotomer pathways that mediate the allosteric communication between subunits. Notably, the perturbed up/down NTD equilibrium in mutant subunits is partially restored by neighboring WT protomers, as is the two-pronged binding of the UBXD1 adaptor that is affected in disease. This work highlights the plasticity of p97 and how subtle perturbations to its free-energy landscape lead to significant changes in NTD conformation and adaptor binding.

p97/VCP | domain cooperativity | protein dynamics | IBMPFD/MSP1 disease mutations | methyl-TROSY

The valosin-containing protein VCP/p97 is a highly conserved and abundant AAA+ (ATPases associated with diverse cellular activities) ATPase that plays an essential role in cellular proteostasis (1–5). VCP/p97 (hereafter referred to as p97) participates in a large number of important cellular activities (6–9), including (*i*) proteasomal degradation, through its roles in extracting proteins from membranes (10, 11) or molecular complexes (12, 13); (*ii*) lysosomal degradation via autophagy (14) and endolysosomal sorting (15–17); (*iii*) membrane fusion (18, 19); and (*iv*) regulation of intracellular signaling (20, 21), cell proliferation, and survival (22). These diverse cellular functions are powered by the chemical energy from ATP hydrolysis (23–25) and coordinated through the interaction of p97 with as many as 40 cofactors that recruit it to specific subcellular locations and to designated substrates for their remodeling and processing.

p97 is organized as a hexameric complex with each subunit (89 kDa) consisting of an N-terminal domain (NTD) followed by two tandem AAA+ ATPase domains, referred to as D1 and D2, that are assembled into a stacked double-ring structure. The NTDs interact with cofactors containing UBX domains (26) or other binding motifs, such as the SHP box (27) and VIM (28). Both X-ray and cryo-EM structures of full-length p97 have revealed that the NTDs exist in one of two different conformations, including a down position in the ADP-bound state in which the NTDs are coplanar with the D1 ring and an up position in the ATP-loaded form in which the NTDs are above the plane of the D1 ring (29, 30) (Fig. 1*A*). It is thought that the up/down equilibrium plays an important functional role in regulating the binding of cofactors (31–33).

The malfunction of p97 has been directly linked to several human degenerative diseases (8, 34). More than 20 missense mutations of the p97 gene have been identified to give rise to an autosomal dominant disorder referred to as inclusion body myopathy associated with Paget disease of bone and frontotemporal dementia (IBMPFD) or as multisystem proteinopathy type 1 (MSP1) (35), which is a severe disorder affecting musculature, bone, and brain function (36). Notably, the majority of these mutations are clustered at the NTD/D1 interface or to the linker between these two domains (34). Solution NMR studies have established that the disease mutations modify the up/down NTD equilibrium in the p97-ADP state, shifting the population from a down conformation that is observed in the WT ADP-loaded protein toward the up state, as observed for WT p97-ATP (37). The extent of the shift correlates with the severity of the disease mutation as well as with the degree of impairment of binding p97 to the UBXD1 adaptor (37), which, in turn, recognizes cargo for lysosomal degradation (15, 38). In this manner, mutations to p97 result in the mislocalization of caveolin in the muscles of patients with IBMPFD by preventing the proper trafficking of this protein to the lysosome, which probably underlies the disease pathogenesis (15). Intriguingly, the perturbed NTD up/down equilibrium in the R155C p97 severe disease mutant could be restored to a near-WT level in vitro by introducing a single compensating point mutation, generating WT-like UBXD1 binding (39).

Previous biophysical studies have shown that the D2 domains of p97 bind and hydrolyze ATP in a cooperative manner and that the cooperativity can be modulated by mutations of residues that affect hydrolysis of nucleotides in the D1 domain (40). In comparison,

Significance

Mutations in the highly conserved hexameric p97 enzyme are associated with a series of diseases affecting muscle, bone, and brain, and have been linked to changes to the orientation of the N-terminal domain (NTD) in each p97 subunit. Although studies have focused on p97 constructs where all protomers are WT or all contain a disease-causing mutation, a strong body of evidence suggests that p97 molecules are heterogeneous, containing a mixture of these subunits in patients. We have used solution NMR to study such heterohexameric structures, showing that the NTD conformation of a disease mutant can be somewhat remedied by WT neighbors, leading to a partial restoration of interactions with adaptor molecules. The mechanism of this allosteric process is investigated.

Author contributions: R.H., Z.A.R., J.L.R., and L.E.K. designed research; R.H. and Z.A.R. performed research; J.L.R. supervised the electron cryomicroscopy studies; R.H., Z.A.R., and L.E.K. analyzed data; and R.H. and L.E.K. wrote the paper.

The authors declare no conflict of interest.

This article is a PNAS Direct Submission.

Published under the PNAS license.

[1]To whom correspondence may be addressed. Email: ruihuangchem@gmail.com or kay@pound.med.utoronto.ca.

This article contains supporting information online at www.pnas.org/lookup/suppl/doi:10.1073/pnas.1815495116/-/DCSupplemental.

Published online December 24, 2018.

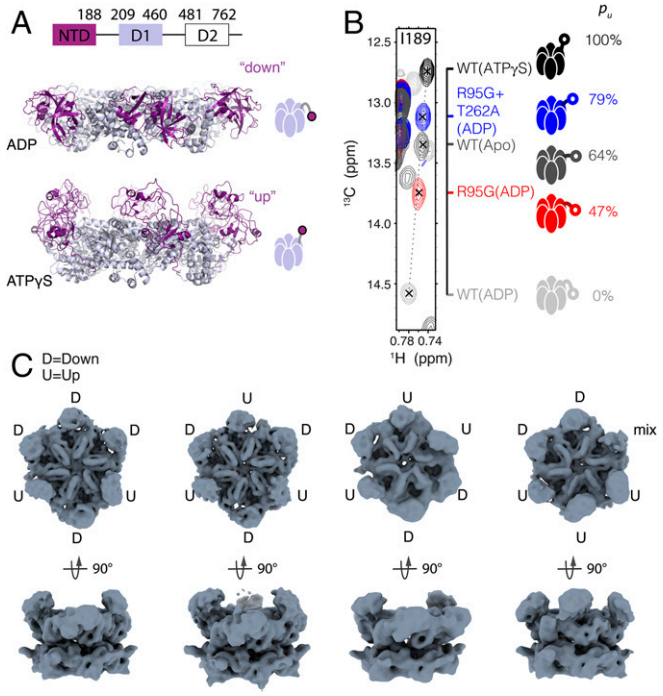

Fig. 1. NTD up/down equilibrium is sensitive to nucleotide state and IBMPFD/MSP1 disease mutations. (*A*) NTDs undergo large-scale domain movement in response to the nucleotide state of D1 (30). (*Top*) Domain organization of each subunit. (*Middle* and *Bottom*) Side views of the ND1L hexamer (NTD in deep purple, D1 in lavender) with ADP (PDB ID code 5FTK) or ATPγS (PDB ID code 5FTN) bound to the D1 domain. Cartoon depictions of ND1L are shown to the right, with a single NTD highlighting the up and down positions. (*B*) Superposition of ^{13}C-^{1}H HMQC subspectra highlighting Ile189 δ1 cross-peaks, indicated by crosshairs, in WT and two disease mutants of p97 ND1L recorded at 18.8 T, 50 °C. The p_u value denotes the fractional population of the NTD up conformation calculated from the peak position of the I189 methyl probe. (*C*) Four representative cryo-EM maps of conformers of ADP-loaded, full-length R95G p97, with NTDs adopting either an up or down conformation in the same hexameric ring.

little is known about whether the up/down motions of NTDs are coupled within a hexameric ring and, if so, what the mechanism of communication between the neighboring NTDs that achieves this might be. Moreover, because IBMPFD is an autosomal dominant disease, patients possess one copy each of both WT and disease mutant alleles, and previous studies provide strong evidence that at least some hexameric complexes of p97 are composed of copies of both gene products (41–43). There is thus considerable interest in understanding how neighboring protomers of one type might influence the up/down NTD equilibrium of a protomer of a second type in these heteromeric complexes and, correspondingly, how binding to the UBXD1 adaptor would be affected in these cases.

Herein, we address these questions using solution NMR methods that exploit a methyl-transverse relaxation optimized spectroscopy (TROSY) effect for studies of high-molecular-weight complexes (44, 45). Notably, we observe the spontaneous formation of p97 heterohexamers composed of both WT and mutant p97 subunits in *Escherichia coli* cells that express both protomers as well as in vitro when homohexameric complexes are mixed, which points to the facile nature by which protomers can exchange between different hexameric particles. Using a 320-kDa single-ring construct of p97 comprising the NTD, D1, and the linker between D1 and D2 as a model system, referred to as ND1L (hexamer with subunit residues 1–480) hereafter, we then explored the cooperativity of the NTD up/down equilibrium by constructing heterohexameric rings of different protomers where only one type of protomer was NMR-observable. Our results establish positive cooperativity between neighboring NTD up/down states, regulated via allosteric coupling with both immediate neighbors of a given protomer. Chemical shift perturbations (CSPs) in NMR spectra further highlight the pathways by which the allostery is communicated between adjacent subunits. Finally, we show that inter-NTD communication can significantly impact function by affecting the binding of UBXD1 adaptor molecules. Our results highlight the intrinsic plasticity of p97 and establish how neighboring protomers can lead to subtle changes in free energies of the up/down states of a mutant protomer that significantly impact the NTD equilibrium and, as a result, adaptor binding.

Results

Solution NMR Studies Quantify the Up/Down NTD Equilibrium. In a previous set of publications, we used the 320-kDa ND1L construct of p97 (6 × 53 kDa) as a model system for structure/function/dynamics studies of a series of IBMPFD mutants leading to different levels of disease severity (37, 39). In these studies, methyl-TROSY–based NMR spectra were recorded on highly deuterated protein samples that were prepared with $^{13}CH_3$ labeling at Ile (δ1), *proR* Leu (δ1), *proR* Val (γ1), and Met (ε1) positions (referred to as U-^{2}H, *proR*,ILVM-$^{13}CH_3$ labeling). For a large number of methyl probes, linear chemical shift titration profiles were observed for different disease mutants in the ADP-loaded form of the protein, as illustrated for Ile189 δ1 in Fig. 1*B*. Ile189 is at the N terminus of the linker connecting the NTD and D1 domains, which undergoes a large conformational change from coil to helix as the NTD transitions from the down conformation to the up conformation (46), and is thus a useful reporter of the status of the up/down NTD equilibrium. In Fig. 1*B*, Ile189 δ1 peaks for the WT ADP and ATPγS states of ND1L [WT(ADP) and WT(ATPγS), respectively] are shown, corresponding to NTDs in the "all down" and "all up" states, respectively (Fig. 1*A*), along with R95G(ADP) and R95G+T262A(ADP) variants and the WT ring in the apo-form (nucleotide-free). Note that in all NMR studies described here, ATPγS, a very slowly hydrolyzing analog of ATP, is used in place of ATP. As described previously, the observed linear correlations of ^{13}C and ^{1}H chemical shifts with different p97 variants can be explained by a rapid two-state interconversion [>15,000 s^{-1} (39)] between up/down conformations of the NTD. The fast equilibrium enables estimation of the relative populations of each state from the positions of reporter cross-peaks relative to the all down [WT(ADP)] and all up [WT(ATPγS)] reference points, as reported by the fractional population of the up state (p_u) in Fig. 1*B*. The severe R95G disease mutation and a combination of the two disease mutations R95G and T262A shift the NTD conformational equilibrium from a completely down state in the ADP-loaded WT enzyme ($p_u = 0$) to $p_u \sim 47\%$ and $p_u \sim 79\%$, respectively, consistent with our previous observations (37). Interestingly, NTDs of apo-WT adopt a predominantly up average conformation ($p_u \sim 64\%$). Similar shifts in peak positions with disease mutation as observed for Ile189 δ1 have been noted for other methyl probes as well (37).

Although the NMR measurements establish both the dynamic nature of the NTDs as well as the relative populations of each interconverting state in the context of a given p97 construct, the measurements are averaged over all hexameric particles in solution, and thus provide no information about the cooperativity of the transition between the two states. We first asked whether the NTD motion was 100% cooperative within a given ring. In this case, one would expect only two structural classes, with either all-up or all-down NTDs. To address this question, we used single-particle cryo-EM to obtain structural models of full-length p97-ADP with the R95G disease mutation. This mutation was selected because $p_u \sim 50\%$, so that in the case of complete cooperativity, equal populations of each state would be realized

that would be easily detected. Initial calculation of a single 3D map showed a symmetrical and relatively rigid AAA+ core comprising the nucleotide-binding domains, allowing structural refinement with symmetry to 3.6-Å resolution. However, with this refinement scheme, the NTD density was fragmented and weak due to the averaging of many different conformations. Three repeated rounds of 3D classification, as described in *SI Appendix*, Fig. S1, revealed the diversity of classes present in the ensemble that differed from one another in the geometric arrangement of NTD positions. Fig. 1*C* shows four representative conformers in which two or three of the six NTDs in the ring are in the up conformation. These structures confirmed that in the R95G disease mutant, the NTD can adopt either an up or down conformation when bound to ADP and that, further, of the NTDs that could be assigned to either the up or down state, ~50% were in each conformation, fully consistent with our NMR observations that establish an interconversion between two equally populated states. The EM structures rule out the possibility of 100% cooperativity for NTD exchange within a given hexamer. We next attempted further 3D classification as, in principle, as many as 14 different conformations of NTDs are expected that are not related to each other by simple rotation about the sixfold symmetry axis of the molecule. These attempts did not lead to robust and accurate quantification, probably due to the limiting signal-to-noise ratio of each particle image, highly skewed fractional populations for certain unlikely configurations (e.g., all-up, all-down), and pseudosymmetry of the complex.

Spontaneous Coassembly of WT and Mutant p97 into Heterohexamers in Vivo and in Vitro. Biophysical studies of IBMPFD disease mutants of p97 have focused on homohexameric structures, whereby each protomer contains the mutation of interest (32, 33, 37, 46–48). However, a significant body of evidence exists in support of the coassembly of endogenous WT p97 and transfection-induced mutant p97 subunits in the amoeba (41) as well as in a human cell line (42, 43). As patients with IBMPFD are heterozygous in p97 alleles (i.e., one WT and one disease), this observation immediately suggests the importance of studies focusing on p97 hexamers containing a mixture of both WT and mutant protomers. To examine the possibility of coassembly of different subunits more quantitatively, we initially carried out experiments testing the formation of heterohexamers when WT and R95G disease mutant p97 protomers are coexpressed in *E. coli*. WT and R95G ND1L were fused with His_6-SUMO–tag (Fig. 2, cyan star) and Strep-tag (Fig. 2, red star), respectively, allowing for differential selection via affinity chromatography. The increased mass of the SUMO-tag relative to the Strep-tag also allows one to distinguish WT from R95G protomers by size on an SDS/PAGE gel. Our results clearly show that a hexameric species composed of a mixture of both WT and R95G protomers (Fig. 2*A*, blue rectangle and *SI Appendix*, Fig. S2) can be purified via binding to both StrepTactin and Ni affinity columns (Fig. 2 *A*, *i* and *ii*), following a procedure that is summarized via the schematic of Fig. 2*B*. While hexamers consisting of only WT or R95G protomers are observed in the flow-through of the two affinity columns (Fig. 2 *A*, *i* and *ii*), their relative concentrations are small, as established by SDS-PAGE, indicating that the majority of the protomers have been incorporated into heterohexameric rings. Controls have been performed to show that Strep-tagged p97 does not bind nonspecifically to Ni affinity resin and, similarly, that His_6-SUMO-p97 elutes in the flow-through from the StrepTactin column (*SI Appendix*, Fig. S2), so that the presence of both SUMO-p97 and Strep-p97 in Fig. 2*A*, *ii* (blue rectangle) indicates that mixing has occurred.

Formation of heterohexamers in vivo could be due to (*i*) translation and subsequent assembly of proximal WT and mutant protomers into a complex, (*ii*) protomer exchange between WT and mutant homohexamers, or (*iii*) a combination of both. We have examined the possibility of subunit interchange by incubating purified His_6-SUMO–tagged WT rings with His_6-less (no tag) R95G hexamers (ratio of 0.30:0.70 in favor of His_6-less; subunits are ND1L) overnight at 37 °C. Copurification of hexamers containing both forms of protomer from a Ni affinity column (Fig. 2*C*) establishes that subunit interchange occurs, as illustrated schematically in Fig. 2*D*. We have carried out a similar experiment using full-length R95G and WT p97 constructs that again shows spontaneous mixing of subunits (Fig. 2*E*).

We further assessed the extent of protomer exchange by quantifying the fractional populations of hexamers without His_6-tags after incubation with varying ratios of WT (His_6-SUMO) and R95G (no His_6-tag) rings for 16 h at 37 °C. Assuming no protomer exchange, the percentage of His_6-less hexamers produced would mirror that of the input His_6-less protomers (R95G p97) (Fig. 2*F*, solid black line). On the other hand, if the two protomer types coassemble randomly into hexamers, the percentage of His_6-less hexamers is expected to follow a curve of the form $y = x^6$, where x is the fraction of the His_6-less protomers and y is the fraction of His_6-less hexamers (Fig. 2*F*, dashed black line). Homogeneous mixing was achieved by unfolding the mixture of His_6-tagged and His_6-less hexamers in guanidine hydrochloride (GdnCl), followed by refolding (Fig. 2*F*, magenta triangles). Spontaneous protomer exchange by simple overnight incubation at 37 °C (i.e., no GdnCl) led to nearly complete mixing in the case of ND1L (Fig. 2*F*, gray circles). Although mixing did occur for full-length p97, the efficiency was reduced under the same conditions (Fig. 2*F*, green circles). This observation is readily explained by the fact that in the full-length hexamer, the buried surface between two neighboring protomers is nearly twice that in the ND1L hexamer, decreasing the probability of protomer dissociation and reincorporation into a different hexamer.

Spontaneous protomer exchange was further confirmed by NMR experiments carried out on U-^{2}H, I-$^{13}CH_3$ R95G and U-^{2}H WT ND1L hexamers that were mixed at a molar ratio of 0.15:0.85 and treated in one of the following two ways: (*i*) unfolding in GdnCl, followed by refolding to facilitate homogeneous mixing, or (*ii*) incubating overnight at 37 °C. Fig. 2*G* superimposes identical regions of ^{13}C-^{1}H heteronuclear multiple-quantum coherence (HMQC) spectra recorded on the two differently prepared samples as well as on an unmixed U-^{2}H, I-$^{13}CH_3$ R95G sample. Note that only the R95G protomers are NMR-visible in the spectra. In sample (*i*), the R95G protomers were dispersed into hexamers mainly composed of WT subunits, with probabilities of 97.75% and 72.25% of at least one or both neighbors being WT, respectively. Notable chemical shift differences between the unmixed, native R95G hexamers (Fig. 2*G*, red) and heterohexamers prepared by scheme (*i*) (Fig. 2*G*, green) are the result of the influence of the neighboring protomers on the chemical environment/conformation of the R95G protomer that is monitored. Of interest, the spectrum recorded of the native mixture of R95G and WT hexamers after overnight incubation (Fig. 2*G*, black) superimposes perfectly with the dataset obtained from the GdnCl-mixed heterohexamers (Fig. 2*G*, green), again confirming spontaneous formation of heterohexameric rings.

A Cooperative Up/Down NTD Equilibrium. Having established that protomers in both ND1L and full-length p97 exchange between hexameric particles in vitro and that p97 molecules with mixed subunit composition are found in vivo, consistent with results from studies involving eukaryotic cells (41–43), we next asked what the implications might be for the up/down NTD equilibrium in the context of a hexamer containing mixed subunits. To this end, we focused on the ND1L construct with hexamers prepared by mixing 15% U-^{2}H, I-$^{13}CH_3$–labeled (Fig. 3*A*, filled ovals, NMR-visible) and 85% U-^{2}H–labeled (Fig. 3*A*, empty ovals, NMR-invisible) protomers via a procedure in which mixtures of different p97 molecules are first unfolded in GdnCl and

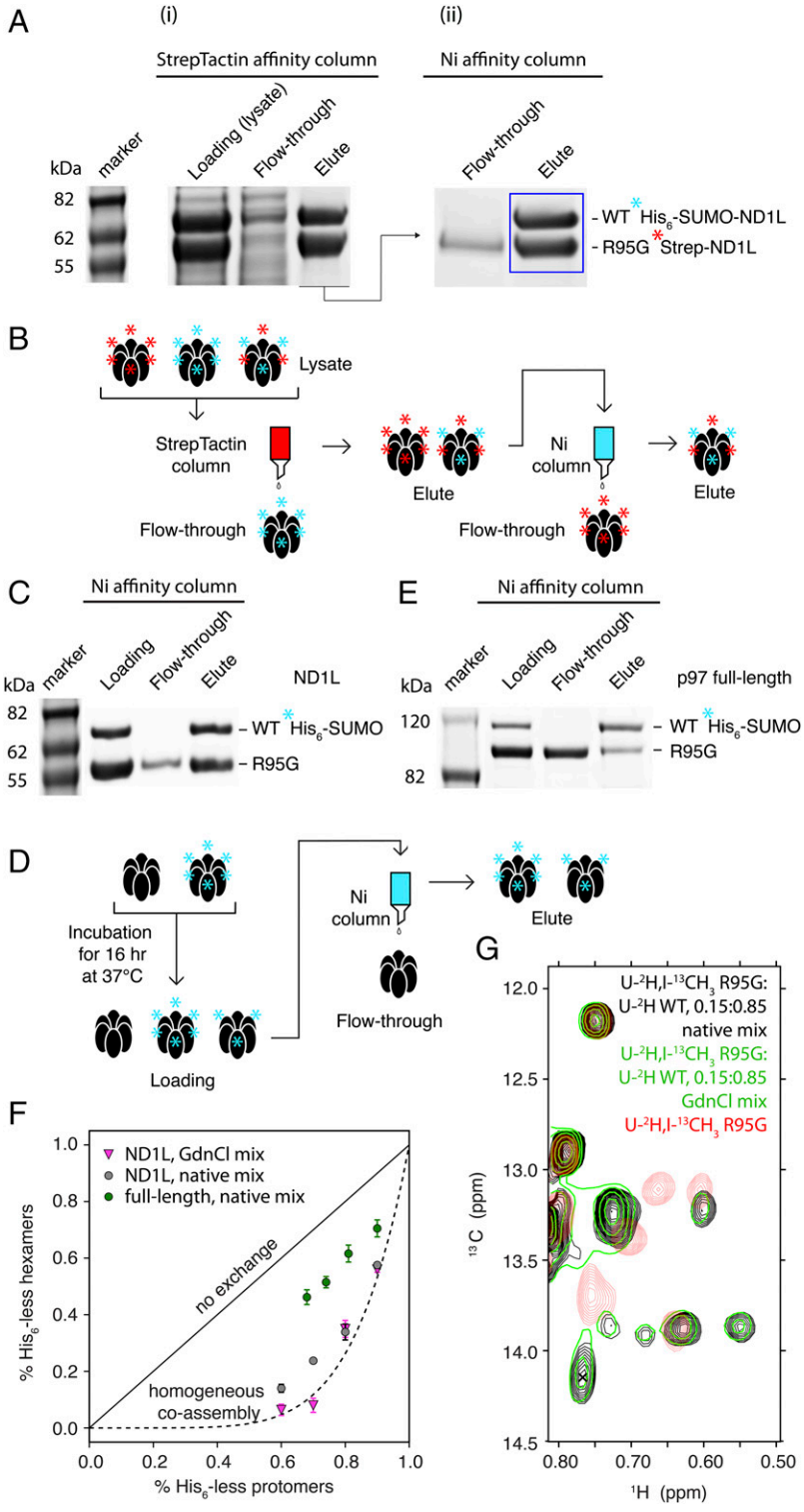

Fig. 2. Spontaneous formation of p97 heterohexamers. (*A*) Coexpression of WT His_6-SUMO (cyan star)-ND1L and R95G Strep (red star)-ND1L constructs results in hexamers of mixed subunit composition, as evidenced by binding to both StrepTactin (*i*) and Ni affinity columns (*ii*, blue rectangle). The readout is by SDS/PAGE gel electrophoresis. (*B*) Procedure used is illustrated in the schematic, and is described in detail in the main text (*Spontaneous Coassembly of WT and Mutant p97 into Heterohexamers in Vivo and in Vitro*). (*C*) Incubation of His_6-SUMO (cyan star)–tagged WT with His_6-less R95G rings in a molar ratio of 0.3:0.7 (ND1L, 16 h at 37 °C) leads to mixing of subunits and copurification of hexamers with both R95G and WT protomers via Ni affinity chromatography. (*D*) Procedure used is illustrated, and is described in detail in the main text (*Spontaneous Coassembly of WT and Mutant p97 into Heterohexamers in Vivo and in Vitro*). (*E*) As in *C*, but with full-length p97 constructs. (*F*) Different ratios of His_6-SUMO-WT and R95G (no tag, His_6-less) homohexamers were unfolded in GdnCl followed by refolding (ND1L, magenta triangles) or natively incubated for 16 h at 37 °C (ND1L, gray circles; full-length p97, green circles), and the percentage of hexamers without the His_6-tag was established via Ni affinity chromatography. The expected correlations for no protomer exchange or random coassembly are shown by the solid ($y = x$) and dashed ($y = x^6$) black lines, respectively. (*G*) Superposition of selected ^{13}C-^{1}H HMQC subspectra (18.8 T, 50 °C) recorded of U-^{2}H, I-$^{13}CH_3$ R95G ND1L (red) and ND1L prepared by unfolding and refolding a 0.15:0.85 U-^{2}H, I-$^{13}CH_3$ R95G/U-^{2}H WT mixture (green) or natively incubating the mixture for 16 h at 37 °C (black).

subsequently refolded. The use of a 0.15:0.85 NMR active/inactive ratio is a compromise to ensure sufficient sensitivity in spectra as well as a strong likelihood that upon mixing subunits A (NMR-visible) and B (NMR-invisible), where the NTDs in A and B can have different p_u values, a high probability of A with B nearest neighbors is achieved. This approach allows the effect of the B subunits on the up/down conformations of NTDs from A protomers to be ascertained directly. We examined three different protomers, including WT, the R95G mutant, and the R95G+T262A double mutant, with one of the subunits U-^{2}H, I-$^{13}CH_3$–labeled and the others U-^{2}H–labeled, to give a total of nine different p97 constructs (all ADP-loaded). These R95G and R95G+T262A mutants were selected based on large CSPs relative to WT p97-ADP for key residues reporting on the up/down equilibrium that could be used, therefore, as reporters of even subtle changes to the NTDs that arise from effects involving neighboring subunits. In Fig. 3 *B*–*D*, a selected region of the ^{13}C-^{1}H HMQC spectrum is presented, highlighting the Ile189

δ1 methyl resonance whose position reports on the up/down equilibrium, with similar trends observed for other methyl reporter probes as well (*SI Appendix*, Fig. S3). In each spectrum in Fig. 3 *B–D*, WT(ADP) and WT(ATPγS) correlations are shown in dashed gray and black single contours, respectively. In Fig. 3*B*, the Ile189 δ1 peak from the R95G subunit (red subunit, NMR-visible) moves progressively upfield as the up/down equilibrium of the neighboring subunits (NMR-invisible) shifts increasingly to the up state (Fig. 1*B*). The p_u values for the NTDs of the R95G subunits increase from 27% for a WT(ADP) background to 82% for the R95G+T262A double-mutant background, while a value of 47% up is measured for a homohexameric R95G structure. A similar situation was observed for the NTD of the R95G+T262A protomer, whereby the up/down equilibrium was also shifted toward that of the neighboring NTDs (Fig. 3*C*). These results highlight the interplay between the positions of the NTDs of disease mutants and those of the NTDs of surrounding subunits. In contrast, in the ADP-loaded state, the NTDs of the WT protomers adopt the down conformation even when adjacent subunits are up (Fig. 3*D*), suggesting that intrasubunit interactions between the NTD and the D1 domain are sufficiently strong to stabilize the conformation of the WT protomer in a manner that appears not to depend on the NTD orientation of the neighbors.

The measured p_u values can be used to calculate differences in free energy (ΔG) values for the up/down equilibrium of a given subunit in different protomer backgrounds, as illustrated schematically by the two-state energy diagrams in Fig. 3*E*. Here, we have assumed, for simplicity and ease of presentation, that the neighbors affect the energies of the NTD down states exclusively; however, in reality, the energies of both up and down conformers could be perturbed. Notably, changes in ΔG ($\Delta\Delta G$) values are small, on the order of 1 kcal/mol or less (Fig. 3 *E*, *i* and *ii*). Nevertheless, the observed positive cooperativity between subunits can result in significant shifts in NTD up/down equilibria for disease mutation-containing protomers, as the populations of the interconverting states are of a similar magnitude in these cases. The small energies required to perturb the equilibrium for mutant p97s are in contrast to the case for WT p97, where the transition from the up conformation to the down conformation requires hydrolysis of ATP (30).

The influence of neighboring subunits on NTD dynamics is further illustrated by a set of experiments performed on heterohexameric particles constructed from 15% U-^{2}H, I-$^{13}CH_3$–labeled WT and 85% U-^{2}H, *proR*,LV–labeled R155C+N387C double-mutant protomers (Fig. 4). In the down conformation, positions 155 and 387 are proximal and Cys residues at these sites can be readily oxidized (37, 39) so as to create a "locked-down" NTD state even after subsequent removal of ADP (*SI Appendix*, Fig. S4). Conversely, addition of reducing agent breaks the "lock" and allows the NTD to adopt a predominantly up conformation in the apo state (*SI Appendix*, Fig. S4), similar to the situation for apo-WT protein (Fig. 1*B*). We quantified the up/down equilibrium in this study as shown in Fig. 3, focusing on the position of the Ile189 δ1 methyl group as a reporter. As expected, the NTDs of the WT subunits (NMR Ile-visible) are in the down conformation in the ADP-loaded form of the protein

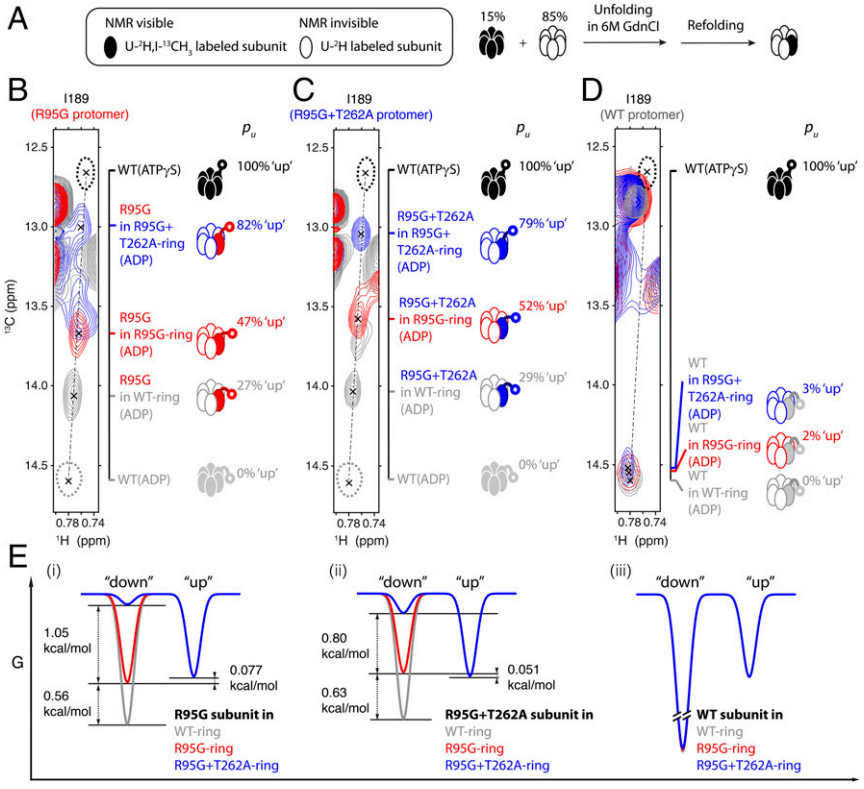

Fig. 3. NTD up/down equilibrium is cooperative. (*A*) Heterohexamers, composed of 15% U-^{2}H, I-$^{13}CH_3$ (NMR-active, filled ovals) and 85% U-^{2}H (NMR-invisible, empty ovals) protomers, are prepared via GdnCl unfolding/refolding. (*B–D*) Superposition of a select region from ^{13}C-^{1}H HMQC spectra (18.8 T, 50 °C) focusing on the Ile189 δ1 methyl correlation (cross-hairs) and recorded on samples whose protomer composition is as indicated. R95G, R95G+T262A, WT protomers are NMR-visible in *B*, *C*, and *D*, respectively. The p_u values of the NTDs, along with schematics of the heterohexamers studied, are shown to the right of the spectra in *B–D*, with WT(ADP), WT(ATPγS), R95G, and R95G+T262A protomers colored in gray, black, red, and blue, respectively. Only a single NTD, that of the NMR-visible protomer, is highlighted. Peak positions of Ile189 in ADP- and ATPγS-loaded U-^{2}H, I-$^{13}CH_3$ WT ND1L are indicated by the dashed gray and dashed black single contours, respectively, and are taken as references for the 0% and 100% up populations of the NTD. (*E*) Two-state, free-energy diagrams showing ΔG values for the up/down equilibrium of a given subunit in different protomer backgrounds, as illustrated.

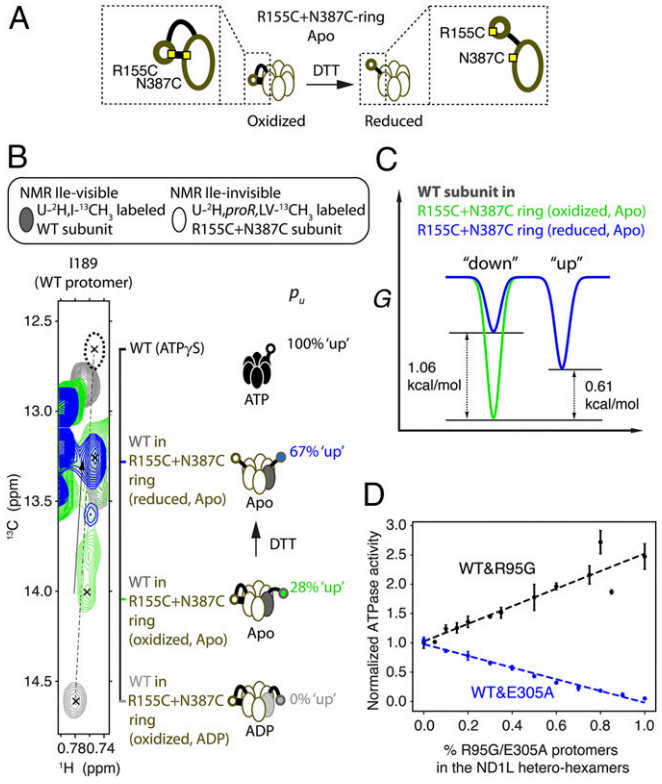

Fig. 4. Apo-WT NTD equilibrium can be shifted by neighboring subunits. (*A*) Schematic of the procedure used to manipulate the NTD up/down conformation in apo-R155C+N387C protomers through disulfide oxidation/reduction. (*B*) Superposition of a selected region of ^{13}C-^{1}H HMQC spectra (18.8 T, 50 °C) recorded on heterohexamers composed of 15% U-^{2}H, I-$^{13}CH_3$–labeled WT and 85% U-^{2}H, *proR*,LV–labeled R155C+N387C protomers under oxidizing (green for the apo state, gray for the ADP state) or reducing (blue) conditions. WT protomers are indicated in the cartoons to the right with varying shades of gray, from light gray to black, while R155C+N387C subunits are white. The p_u values for the WT subunits are shown. (*C*) Two-state, free-energy diagram for the up/down NTD equilibrium of the apo-WT subunit when surrounded by oxidized R155C+N387C (green) or reduced R155C+N387C protomers (blue). (*D*) Normalized ATPase activities of ND1L hexamers with different fractions of WT and R95G protomers (black circles) or WT and Walker B mutant E305A subunits (blue circles). ATPase activities vary linearly with the fraction of R95G/E305A subunits, as indicated by the dashed lines.

when the surrounding protomers are locked down (Fig. 4*B*, gray cross-peak, $p_u = 0\%$). Recall that a similar down conformation is also observed for WT-ADP subunits in the context of a homohexameric particle (Fig. 1*B*). However, upon removal of ADP, a p_u value of 28% was measured for the WT NTDs that are doped in oxidized R155C+N387C rings (i.e., NTDs in the locked down conformation) where all subunits are apo (Fig. 4*B*, green spectrum); p_u increased to 67% upon "unlocking" the NTDs of the neighboring protomers under reducing conditions (Fig. 4*B*, blue spectrum), a value similar to that obtained for homohexameric rings composed of WT(Apo) protomers exclusively (Fig. 1*B*). The shift in the equilibrium corresponds to a $\Delta\Delta G$ of 1.06 kcal/mol (Fig. 4*C*).

We were also interested in establishing whether the cooperativity observed between neighboring NTDs extends to ATP hydrolysis as well. To this end, samples were prepared with different fractions of WT ND1L and disease mutant R95G or E305A subunits. The E305A Walker B mutation prevents ATP hydrolysis, while allowing nucleotide binding to occur (49). In contrast, the hydrolysis rate is ~2.5-fold faster than WT for the R95G homohexamer (Fig. 4*D*). Samples with a range of WT/mutant protomer ratios were prepared, using the GdnCl mixing approach described above, and ATPase activities were measured. Notably, the activities are linearly correlated with the fraction of mutant protomers in the heterohexamers (Fig. 4*D*), suggesting that hydrolysis of ATP in each protomer of D1 is largely independent of the hydrolysis rates in the surrounding subunits. Finally, in a series of controls, we show that the GdnCl-assisted unfolding/refolding approach used in this study does not lead to changes in structure or in the relative up/down NTD equilibrium, as NMR spectra of ADP-loaded homohexameric R95G ND1L rings and R95G rings generated by protomer unfolding/refolding are superimposable (*SI Appendix*, Fig. S5). Fig. 2*G* provides further support that the p97 structure is not affected by GdnCl unfolding/folding as both the native and GdnCl mix spectra superimpose. Comparative ATP hydrolysis assays on samples prepared with or without the refolding protocol establish that the ATPase activity of the enzyme is also not affected by the mixing protocol (*SI Appendix*, Fig. S5).

A Structural Basis for NTD Cooperativity. In an effort to obtain structural insights into how the NTD up/down equilibrium is affected by adjacent subunits, we prepared a heterohexameric ND1L sample comprising 15% U-^{2}H, IM-$^{13}CH_3$–labeled WT (NMR-visible) and 85% U-^{2}H–labeled R95G (NMR-invisible) protomers in the ADP state, using the GdnCl unfolding/refolding method. A second sample of U-^{2}H, IM-$^{13}CH_3$–labeled WT ND1L in the ADP-loaded form was prepared for comparison. Fig. 5*A* plots the CSPs quantified by comparing spectra of these two samples, reflecting changes in the WT protomers from neighbors that are either interconverting between up and down conformers (sample 1) or in the all down position (sample 2). Note that the up/down NTD equilibrium of a WT-ADP protomer is not influenced by neighboring subunits (Fig. 3*D*), so that the observed CSPs in spectra of WT subunits report only on changes that arise from interprotomer communication. Residues with significant perturbations (CSP of 1 SD above the mean, indicated by the black solid line in Fig. 5*A*) are located at interfaces between the protomer of interest and both of its neighbors, the positions of which are shown on a structure of p97 (Fig. 5*B*, *Right*, red spheres). Notably, residues Met427, Ile430, and Ile437 are clustered in a region of D1 bridging both the NTD of the same protomer (Fig. 5*B*, purple) and a short helix in the D1 of the neighboring protomer (Fig. 5*B*, gray), while Ile233 forms contacts with the D1 (Fig. 5*B*, gray) and the NTD of the second neighboring protomer (Fig. 5*B*, cyan). These regions are likely important for the allosteric pathways that connect neighboring NTDs and that lead to the cooperative up/down equilibrium.

Having identified two potential intersubunit pathways connecting an NTD with its neighboring protomers, we next asked whether both of the neighbors play a role in influencing the NTD up/down equilibrium of the middle protomer. To address this question, titration experiments were performed in which the molar ratios of U-^{2}H–labeled WT: U-^{2}H, I-$^{13}CH_3$–labeled R95G (A) or R95G+T262A (B) protomers were varied in ADP-loaded heterohexamers. Fig. 6 shows a series of NMR spectra corresponding to titration points for WT/R95G and WT/R95G+T262A heterohexamers focusing on residues Ile189 and Ile274, respectively. At the start of the titrations, where samples are 10% and 16% in R95G and R95G+T262A (NMR-active) subunits, respectively, 81.0% and 70.6% of the NMR-active (i.e., mutant) protomers are flanked by WT (i.e., NMR-inactive) subunits, so that peak positions report mainly on the case where protomers have WT neighbors exclusively (Fig. 6, gray dashed lines). In contrast, at the end of each titration, where spectra of either R95G or R95G+T262A homohexamers are recorded (Fig. 6 *A*, *vii* and *B*, *v*), each NMR-active subunit is surrounded by similarly mutated protomers (Fig. 6 *A*, red dashed line and *B*, blue dashed line). Notably, during the course of each titration, a third peak

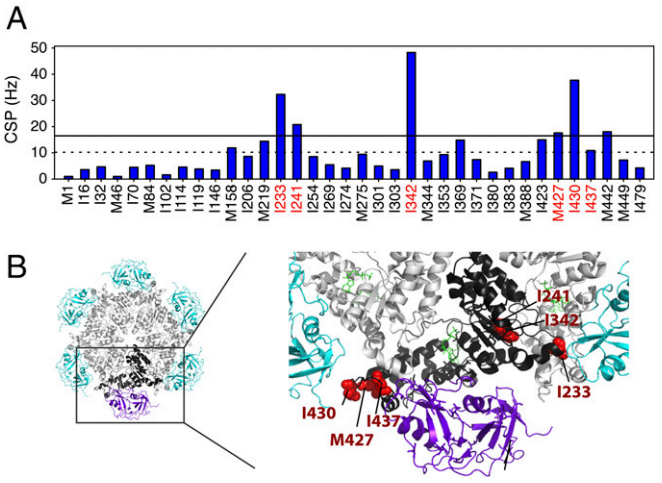

Fig. 5. Mapping interprotomer pathways connecting neighboring NTDs. (*A*) CSPs quantified between spectra of hexamers composed of 15% U-^{2}H, IM-^{13}CH$_3$–labeled WT and 85% U-^{2}H–labeled R95G protomers in the ADP state and hexamers of U-^{2}H, IM-^{13}CH$_3$–labeled WT ND1L in the ADP-loaded form. The average CSP is indicated by the dashed black line; residues with CSPs 1 SD or more above the average (solid black line) are highlighted in red. CSP = $\{(\Delta\nu H)^2 + (\Delta\nu C)^2\}^{0.5}$, where $\Delta\nu$H and $\Delta\nu$C are ^{1}H and ^{13}C chemical shift differences (hertz), respectively. (*B*, *Left*) Top view of the WT-p97 structure in the ADP state (PDB ID code 5FTK), with the NTD and D1 of one of the protomers colored in purple and black, respectively. (*B*, *Right*) Enlarged region focusing on this protomer, with residues displaying significant CSPs in *A* shown as red spheres. Other Ile and Met residues in the protomer are displayed as sticks, and the ADP is colored green.

appeared between the two end-point resonances, subsequently disappearing as the fraction of mutant subunit increased (Fig. 6, green dashed lines). These resonances most likely arise from mutant protomers with only a single WT neighbor. Thus, our titration data are consistent with both neighboring subunits influencing the NTD up/down equilibrium, as suggested by the CSP experiments of Fig. 5 that show pathways connecting a subunit with both nearest neighbors.

Functional Implications for Adaptor Binding. As a next step, we were interested in evaluating how the cooperative network affecting NTD up/down equilibria influences adaptor binding. Among the many adaptors of p97 is UBXD1, which recruits it for sorting of ubiquitylated cargo via the lysosomal pathway (15, 38). This function is impaired by IBMPFD disease mutations, such as R95G and T262A (15), that have been considered in the present study. Previously, we demonstrated that an N-terminal fragment of UBXD1 (UBXD1N, residues 1–133) interacts with WT-ADP p97 via a two-pronged mechanism whereby (*i*) the canonical p97 interacting motif, VIM (residues 52–63), of UBXD1 docks on the NTD of p97 and (*ii*) the H1/H2 region (residues 1–25) of UBXD1 binds to the p97 NTD/D1 interface (37). A schematic of this two-pronged binding interaction is shown in Fig. 7*A*.

Previous NMR studies of binding of UBXD1 to p97-ADP showed that disease mutations of increasing severity progressively disrupt the interaction between the UBXD1 H1/H2 motif and the p97 NTD/D1 interface (37, 39) to the point where, in the case of homohexamers containing the R95G severe disease mutation, this contact is no longer formed (i.e., one of the two prongs does not interact). We illustrate this reduced binding in Fig. 7*B* to set the stage for understanding subsequent binding experiments using heteromeric complexes. In Fig. 7*B*, a superposition of spectral regions of ADP-loaded, U-^{2}H, *proR*, ILVM-^{13}CH$_3$–labeled R95G ND1L without (green) and with (purple) 1 molar eq of UBXD1N is presented, focusing on Val68, Ile175, Ile146, and Ile189 of p97. Val68 and Ile175 are located in the VIM docking site localized to a hydrophobic pocket between the two subdomains of the NTD (37, 50), while

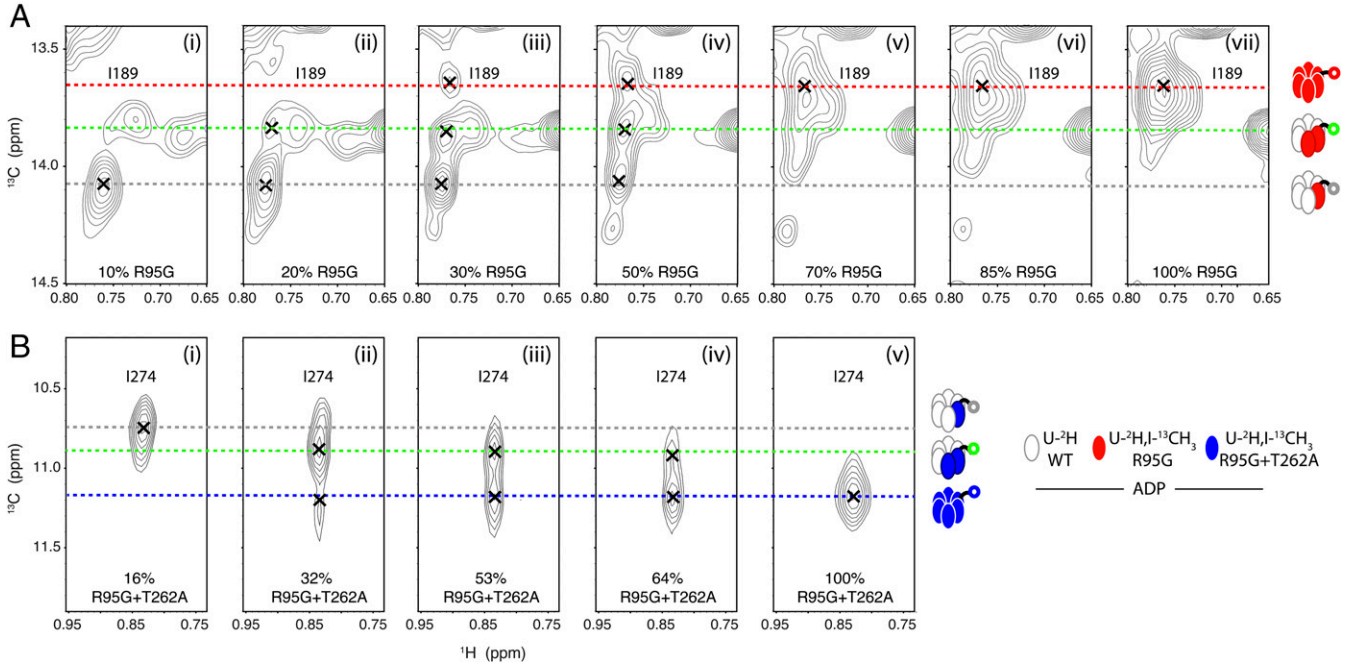

Fig. 6. NTD up/down equilibrium of a subunit is affected by both neighboring protomers. (*A*) Selected region of ^{13}C-^{1}H spectra (18.8 T, 50 °C) recorded on a series of samples of heterohexamers composed of U-^{2}H, I-^{13}CH$_3$–labeled R95G and U-^{2}H–labeled WT ND1L protomers at different molar ratios, with the fraction of R95G protomers indicated. Correlations of I189, denoted by cross-hairs, show three distinct positions during the titration, marked by gray, green, and red dashed lines, reporting on the up/down equilibrium of an NTD when it has two, one, or zero WT neighbors, respectively. (*B*) As in *A*, but with U-^{2}H, I-^{13}CH$_3$–labeled R95G+T262A protomers replacing the R95G subunits and focusing on the Ile274 δ1 methyl. All spectra were recorded in the ADP state.

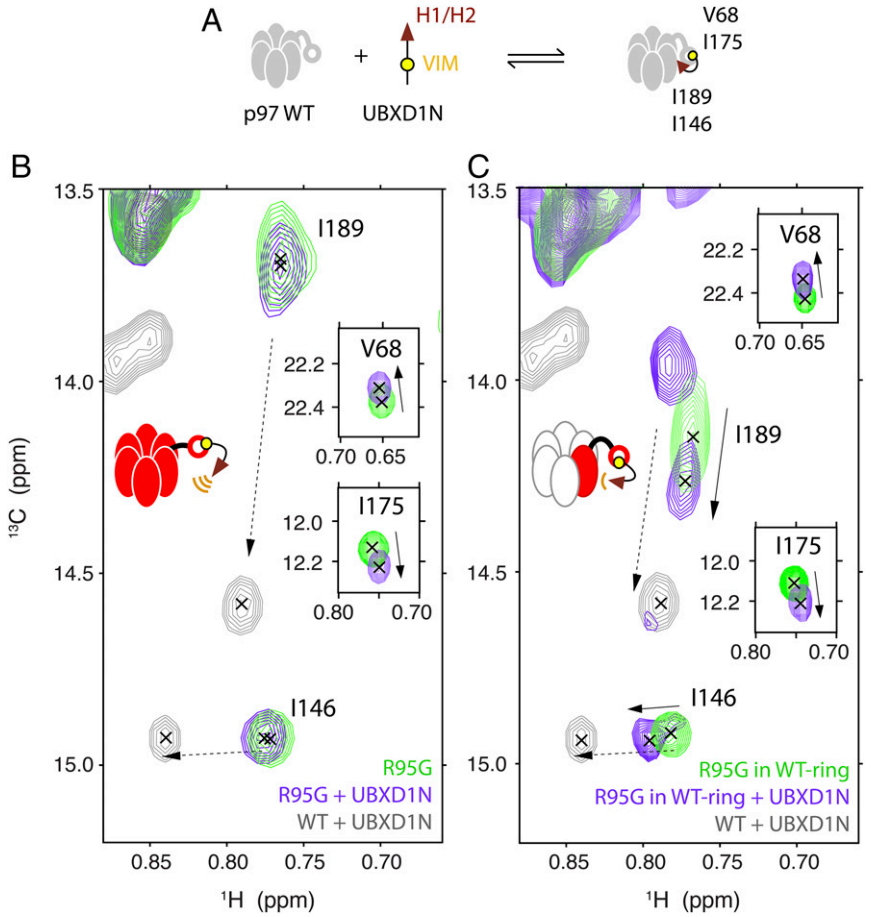

Fig. 7. Allostery between neighboring NTDs affects UBXD1 adaptor binding. (*A*) Schematic of the two-pronged UBXD1N (residues 1–133) and WT p97-ND1L binding; Val68 and Ile175 are reporters of VIM binding, while Ile146 and Ile189 are sensitive to the interaction involving H1/H2. (*B*) Selected regions of ^{13}C-^{1}H HMQC spectra (18.8 T, 50 °C) of U-^{2}H, *proR*,ILVM–labeled R95G ND1L homohexamers in the absence (green) and presence (purple) of 1 molar eq of UBXD1N. (*C*) As in *B*, but with U-^{2}H, *proR*,ILVM–labeled R95G protomers mixed with U-^{2}H WT protomers at a ratio of 0.15:0.85 (via GdnCl unfolding/folding). Partial two-pronged binding of UBXD1N is restored, as indicated by the CSPs of residues Val68 and Ile175 (binding of the VIM motif) as well as residues of Ile146 and Ile189 (binding of the H1/H2 region). Cross-peaks of Ile146 and Ile189 from spectra of WT ND1L bound with UBXD1N are shown as a reference in gray. Spectra were recorded in the ADP state.

Ile146 and Ile189 report on the up/down NTD equilibrium, and hence on the interaction between the UBXD1 H1/H2 motif and the p97 NTD/D1 interface (37). Although binding of the VIM domain to the NTDs of p97 does occur, as shown by the change in Val68 and Ile175 peak positions upon addition of UBXD1N (Fig. 7*B*, *Insets*), there is no shift in peaks derived from Ile146 and Ile189 (Fig. 7*B*), indicating that the second prong of the interaction involving the H1/H2 domain cannot form. For reference, the positions of Ile146 and Ile189 methyl peaks in a complex of UBXD1N with the WT ND1L protein, where the second prong is present, are highlighted in gray.

A second set of samples of ADP-loaded ND1L was prepared consisting of 15% U-^{2}H, *proR*,ILVM-$^{13}CH_3$–labeled R95G (NMR-visible) and 85% U-^{2}H–labeled WT (NMR-invisible) protomers without and with an equal molar ratio of UBXD1N to p97 protomer. The labeling used in the present study ensures that only binding of adaptor to R95G mutant protomers is observed in the spectra. Based on the fact that neighboring WT protomers can partially restore the up/down equilibrium of R95G subunits to a more WT-like down conformation (Fig. 3*B*), it would be expected that binding of UBXD1 to R95G protomers in heterohexamers would be more WT-like compared with the situation where all subunits are R95G, with at least a partial two-pronged interaction expected. That this is the case is illustrated in Fig. 7*C*, where methyl peaks from Val68 and Ile175 reposition upon addition of UBXD1N (Fig. 7*C*, *Insets*), with partial movement of correlations derived from Ile146 and Ile189 (Fig. 7*C*, purple peaks) toward a locked-down conformation (Fig. 7*C*, gray peaks) that is characteristic of the NTD/D1–H1/H2 interaction in the WT ND1L–UBXD1N complex. Thus, the allostery between neighboring NTDs that influences the up/down equilibrium in disease mutant protomers, in turn, affects adaptor binding.

Discussion

p97 is indispensable for a diverse array of cellular processes, including protein degradation, desegregation of components from complexes, membrane fusion, DNA repair, and intracellular signaling (8, 18, 51–53). Missense mutations in p97 are associated with human diseases termed IBMPFD or, more recently, MSP1, which are characterized by progressive muscle/bone weakness as well as neurodegeneration (35, 36). IBMPFD/MSP1 is an autosomal dominant disease in which patients have a single WT copy and one disease-mutated copy of the p97 allele (34, 54), and there is a wealth of biochemical evidence to suggest that p97 hexamers contain mixtures of WT and mutant subunits. For example, in studies involving expression of both disease mutant and endogenous WT p97 in transformed/transfected *Dictyostelium discoideum* (41) and the U2OS human cell line (42, 43), it was found that endogenous WT p97 coassembles into

heteromeric complexes with disease mutant subunits. Disease is not the result of reduced levels of the WT protein, as knockout mice retaining a single copy of the WT allele ($p97^{+/-}$) can develop to normal size and fertility, indistinguishable from mice with both alleles intact (5). Corroborating these observations, we have shown in the current study that coexpression of WT and disease mutant p97 protomers in *E. coli* led to the formation of heterohexamers (Fig. 2*A*). Notably, these could also be formed spontaneously in vitro from a mixture of WT and mutant homohexameric structures via subunit exchange (Fig. 2 *C*–*E*).

Most in vitro studies of p97 to date have been performed on homooligomeric complexes composed of only a single protomer type (either WT or a mutant) (32, 33, 37, 46–48), and it is of interest to establish how the structural dynamics of the heterohexamers that exist in patients with disease might differ. Therefore, we constructed p97 heterohexamers consisting of uniquely isotopically labeled WT and disease mutant protomers, allowing different protomer types in a ring to be investigated independently by a methyl-TROSY–based NMR method that enables quantitative studies of molecular machines (44, 45). Such an approach has been successfully implemented in our previous work investigating the cooperativity of proteasome gating (55) as well as allostery in the ClpP protease (24). Here, a 320-kDa ND1L construct of p97 was used as a model system for structural studies, since we showed previously that the shorter construct faithfully reproduces methyl chemical shift changes observed in full-length p97 in a series of IBMPFD disease mutants (37), while improving the quality of spectra, especially with respect to crowding.

The work described in this report builds upon previous observations that in ADP-loaded p97, the NTD up/down equilibrium becomes progressively perturbed toward the up state as a function of disease severity (37). Using a series of different heterohexameric p97 constructs comprising either combinations of WT and mutant subunits (all ADP-loaded; Fig. 3 *B*–*D*) or WT and R155C+N387C protomers that are cross-linked so as to form a locked-down state (no nucleotides; Fig. 4), we show that the NTD up/down equilibrium is cooperative. NMR spectra focusing on methyl probes that report on the relative fractions of rapidly exchanging NTD up/down states clearly show that NTD up/down conformations of both mutant (ADP-loaded) and apo-WT subunits shift toward those of neighboring NTDs (Figs. 3 *B* and *C* and 4*B*). Interestingly, NTDs of ADP-WT protomers are not perturbed from their down conformations even when the surrounding NTDs are all up (Fig. 3*D*). The high stability of the down conformation for an ADP-WT subunit likely originates from the abundant contacts between the NTD and D1 in the down state (*SI Appendix*, Fig. S6) with a larger interdomain interface (~2,130 Å^2, calculated from PDB ID code 5FTK) compared with that in the up state (ATPγS-WT) (~882 Å^2, calculated from PDB ID code 5FTN). Disease mutations localized to regions of interdomain contacts destabilize the down conformation in the ADP state, so that the position of the NTD equilibrium can be affected via cooperative interactions involving neighbors. By comparing chemical shift changes between spectra of an ADP-WT subunit in homohexameric (all WT) and heterohexameric (WT/R95G = 0.15:0.85) p97 samples, key residues that form interprotomer contacts between NTD and D1 domains have been identified. As position 95 is not proximal to the interface between subunits, the observed CSPs are not the direct result of the mutation per se, but rather identify allosteric pathways of communication between subunits (Fig. 5). Further, titration experiments whereby disease mutation-containing protomers, either R95G or R95G+T262A, are mixed with WT subunits show that both immediate neighbors affect the NTD state of the R95G or R95G/T262A protomer (Fig. 6). The functional importance of NTD cooperativity is underscored by its implications for UBXD1 adaptor binding. The presence of neighboring WT subunits leads to a shift in the up/down NTD equilibrium toward the down state for a mutant subunit and, in turn, a partial restoration of the two-pronged UBXD1-p97 binding at that site (Fig. 7). Interestingly, in the context of the R95G protomer, the presence of adjacent WT subunits shifts p_u to a similar value as obtained for the R155H mild disease mutant ($p_u \sim 15\%$), where partial two-pronged UBXD1 binding was also observed (37). When the up/down equilibrium was further shifted almost completely to the down state in a severe R155C p97 disease mutant, through a single amino acid substitution (39), WT binding of UBXD1 was restored. Taken together, data presented here and elsewhere (37, 39) establish a link between a shift in the up/down NTD conformation toward that of the WT and an increase in binding of UBXD1 that reflects strengthened interactions between the UBXD1 H1/H2 motif and the p97 NTD/D1 interface.

p97 is a highly dynamic molecular machine with functional motions over a broad range of time scales. These include the up/down dynamics of the NTDs, occurring at a rate greater than 15,000 s^{-1} for the R95G mutant (39), as established by a combined analysis of relaxation dispersion data and methyl chemical shift changes between the up and down NTD conformations. The analysis of these data also indicates slower millisecond dynamics for residues at the NTD/D1 domain interface (37, 39). The plasticity of p97 is further underscored by the fact that the NTD up/down equilibrium can be manipulated by introducing point mutations at critical positions in the structure. For example, as described above, addition of the N387C compensating mutation restored the NTD position in an R155C disease mutant to a nearly WT down position (39), while addition of the T262A mutation increased the up conformation of the NTDs of R95G ND1L from 50 to 80% (Fig. 1). Finally, the inherent domain plasticity is also established by the observed subunit exchange among p97 hexamers (Fig. 2), where stabilizing interactions must be broken and then reformed. As expected, the rate of subunit exchange is more rapid for ND1L relative to full-length p97 (Fig. 2), reflecting the much larger interprotomer interface for the full-length protein (~6,800 Å^2 for each of the two interfaces) compared with that for the ND1L construct (~3,420 Å^2). This additional layer of dynamics may be of functional relevance. Cryo-EM studies of the archaeal homolog of p97, VAT, which has 45% sequence identity with p97, suggest a processive hand-over-hand substrate unfolding mechanism whereby each VAT subunit disengages and subsequently reengages along the target protein to facilitate its unfolding (56). Therefore, in the functional VAT hexamer, subunits cannot be rigidly fixed; rather, they must be able to change position during the catalytic cycle. The exchange observed here may therefore be a direct manifestation of the requirement for subunits to partially extricate from the hexameric structure during function.

The NTD up/down cooperativity demonstrated in this study originates from small changes to free-energy landscapes involving less than ~1 kcal/mol that are caused by neighboring protomers. Solution NMR measurements can thus be exquisitely sensitive to subtle, yet important, perturbations, placing NMR in a unique position of connecting high-resolution structures of molecular machines obtained from X-ray and cryo-EM with function through characterization of molecular dynamics.

Materials and Methods

All NMR experiments were performed on a Bruker Avance III HD 18.8-T spectrometer equipped with a cryogenically cooled, pulse-field gradient, triple-resonance probe. The ^{13}C-^{1}H HMQC spectra were recorded at 50 °C (p97-ADP) or 40 °C (apo-p97). All spectra were acquired with an interscan delay of 1.5 s; carriers positioned in the centers of the ^{13}C and ^{1}H spectra regions; and acquisition times of 22 ms and 64 ms in the t_1 and t_2 dimensions, respectively. Additional information concerning preparation of samples for NMR, cryo-EM, and biochemical analyses is provided in *SI Appendix*.

ACKNOWLEDGMENTS. Titan Krios cryo-EM data were collected at the Toronto High-Resolution High-Throughput cryo-EM facility, supported by

the Canadian Foundation for Innovation and the Ontario Research Fund. This work was supported by grants (to L.E.K. and J.L.R.) from the Canadian Institutes of Health Research (CIHR) and the Natural Sciences and Engineering Research Council of Canada. Z.A.R. acknowledges a CIHR postgraduate scholarship, and R.H. is a CIHR postdoctoral fellow. L.E.K. and J.L.R. hold Canada Research Chairs.

1. Fröhlich KU, et al. (1991) Yeast cell cycle protein CDC48p shows full-length homology to the mammalian protein VCP and is a member of a protein family involved in secretion, peroxisome formation, and gene expression. *J Cell Biol* 114:443–453.
2. Lamb JR, Fu V, Wirtz E, Bangs JD (2001) Functional analysis of the trypanosomal AAA protein TbVCP with trans-dominant ATP hydrolysis mutants. *J Biol Chem* 276: 21512–21520.
3. Yamanaka K, Okubo Y, Suzaki T, Ogura T (2004) Analysis of the two p97/VCP/Cdc48p proteins of Caenorhabditis elegans and their suppression of polyglutamine-induced protein aggregation. *J Struct Biol* 146:242–250.
4. León A, McKearin D (1999) Identification of TER94, an AAA ATPase protein, as a Bam-dependent component of the Drosophila fusome. *Mol Biol Cell* 10:3825–3834.
5. Müller JMM, Deinhardt K, Rosewell I, Warren G, Shima DT (2007) Targeted deletion of p97 (VCP/CDC48) in mouse results in early embryonic lethality. *Biochem Biophys Res Commun* 354:459–465.
6. Meyer H, Bug M, Bremer S (2012) Emerging functions of the VCP/p97 AAA-ATPase in the ubiquitin system. *Nat Cell Biol* 14:117–123.
7. Yamanaka K, Sasagawa Y, Ogura T (2012) Recent advances in p97/VCP/Cdc48 cellular functions. *Biochim Biophys Acta* 1823:130–137.
8. Ye Y, Tang WK, Zhang T, Xia D (2017) A mighty "protein extractor" of the cell: Structure and function of the p97/CDC48 ATPase. *Front Mol Biosci* 4:39.
9. Stolz A, Hilt W, Buchberger A, Wolf DH (2011) Cdc48: A power machine in protein degradation. *Trends Biochem Sci* 36:515–523.
10. Shcherbik N, Haines DS (2007) Cdc48p(Npl4p/Ufd1p) binds and segregates membrane-anchored/tethered complexes via a polyubiquitin signal present on the anchors. *Mol Cell* 25:385–397.
11. Tanaka A, et al. (2010) Proteasome and p97 mediate mitophagy and degradation of mitofusins induced by Parkin. *J Cell Biol* 191:1367–1380.
12. Ramadan K, et al. (2007) Cdc48/p97 promotes reformation of the nucleus by extracting the kinase Aurora B from chromatin. *Nature* 450:1258–1262.
13. Verma R, Oania R, Fang R, Smith GT, Deshaies RJ (2011) Cdc48/p97 mediates UV-dependent turnover of RNA Pol II. *Mol Cell* 41:82–92.
14. Ju JS, Weihl CC (2010) p97/VCP at the intersection of the autophagy and the ubiquitin proteasome system. *Autophagy* 6:283–285.
15. Ritz D, et al. (2011) Endolysosomal sorting of ubiquitylated caveolin-1 is regulated by VCP and UBXD1 and impaired by VCP disease mutations. *Nat Cell Biol* 13:1116–1123.
16. Zehner M, et al. (2011) Mannose receptor polyubiquitination regulates endosomal recruitment of p97 and cytosolic antigen translocation for cross-presentation. *Proc Natl Acad Sci USA* 108:9933–9938.
17. Ramanathan HN, Ye Y (2012) The p97 ATPase associates with EEA1 to regulate the size of early endosomes. *Cell Res* 22:346–359.
18. Rabouille C, Levine TP, Peters JM, Warren G (1995) An NSF-like ATPase, p97, and NSF mediate cisternal regrowth from mitotic Golgi fragments. *Cell* 82:905–914.
19. Otter-Nilsson M, Hendriks R, Pecheur-Huet EI, Hoekstra D, Nilsson T (1999) Cytosolic ATPases, p97 and NSF, are sufficient to mediate rapid membrane fusion. *EMBO J* 18: 2074–2083.
20. Alexandru G, et al. (2008) UBXD7 binds multiple ubiquitin ligases and implicates p97 in HIF1α turnover. *Cell* 134:804–816.
21. Hänzelmann P, Schindelin H (2016) Structural basis of ATP hydrolysis and intersubunit signaling in the AAA+ ATPase p97. *Structure* 24:127–139.
22. Haines DS (2010) p97-containing complexes in proliferation control and cancer: Emerging culprits or guilt by association? *Genes Cancer* 1:753–763.
23. Dreveny I, et al. (2004) p97 and close encounters of every kind: A brief review. *Biochem Soc Trans* 32:715–720.
24. Vahidi S, et al. (2018) Reversible inhibition of the ClpP protease via an N-terminal conformational switch. *Proc Natl Acad Sci USA* 115:E6447–E6456.
25. Yeung HO, et al. (2008) Insights into adaptor binding to the AAA protein p97. *Biochem Soc Trans* 36:62–67.
26. Schuberth C, Buchberger A (2008) UBX domain proteins: Major regulators of the AAA ATPase Cdc48/p97. *Cell Mol Life Sci* 65:2360–2371.
27. Isaacson RL, et al. (2007) Detailed structural insights into the p97-Npl4-Ufd1 interface. *J Biol Chem* 282:21361–21369.
28. Ballar P, Shen Y, Yang H, Fang S (2006) The role of a novel p97/valosin-containing protein-interacting motif of gp78 in endoplasmic reticulum-associated degradation. *J Biol Chem* 281:35359–35368.
29. Zhang X, et al. (2000) Structure of the AAA ATPase p97. *Mol Cell* 6:1473–1484.
30. Banerjee S, et al. (2016) 2.3 Å resolution cryo-EM structure of human p97 and mechanism of allosteric inhibition. *Science* 351:871–875.
31. Bodnar NO, Rapoport TA (2017) Molecular mechanism of substrate processing by the Cdc48 ATPase complex. *Cell* 169:722–735.
32. Rao MV, Williams DR, Cocklin S, Loll PJ (2017) Interaction between the AAA+ ATPase p97 and its cofactor ataxin3 in health and disease: Nucleotide-induced conformational changes regulate cofactor binding. *J Biol Chem* 292:18392–18407.
33. Bulfer SL, Chou TF, Arkin MR (2016) p97 disease mutations modulate nucleotide-induced conformation to alter protein-protein interactions. *ACS Chem Biol* 11: 2112–2116.
34. Tang WK, Xia D (2016) Mutations in the human AAA+ chaperone p97 and related diseases. *Front Mol Biosci* 3:79.
35. Watts GDJ, et al. (2004) Inclusion body myopathy associated with Paget disease of bone and frontotemporal dementia is caused by mutant valosin-containing protein. *Nat Genet* 36:377–381.
36. Weihl CC, Pestronk A, Kimonis VE (2009) Valosin-containing protein disease: Inclusion body myopathy with Paget's disease of the bone and fronto-temporal dementia. *Neuromuscul Disord* 19:308–315.
37. Schuetz AK, Kay LE (2016) A Dynamic molecular basis for malfunction in disease mutants of p97/VCP. *eLife* 5:e20143.
38. Madsen L, et al. (2008) Ubxd1 is a novel co-factor of the human p97 ATPase. *Int J Biochem Cell Biol* 40:2927–2942.
39. Schütz AK, Rennella E, Kay LE (2017) Exploiting conformational plasticity in the AAA+ protein VCP/p97 to modify function. *Proc Natl Acad Sci USA* 114:E6822–E6829.
40. DeLaBarre B, Christianson JC, Kopito RR, Brunger AT (2006) Central pore residues mediate the p97/VCP activity required for ERAD. *Mol Cell* 22:451–462.
41. Arhzaouy K, et al. (2012) Heteromeric p97/p97R155C complexes induce dominant negative changes in wild-type and autophagy 9-deficient Dictyostelium strains. *PLoS One* 7:e46879.
42. Weihl CC, Dalal S, Pestronk A, Hanson PI (2006) Inclusion body myopathy-associated mutations in p97/VCP impair endoplasmic reticulum-associated degradation. *Hum Mol Genet* 15:189–199.
43. Dalal S, Rosser MF, Cyr DM, Hanson PI (2004) Distinct roles for the AAA ATPases NSF and p97 in the secretory pathway. *Mol Biol Cell* 15:637–648.
44. Tugarinov V, Hwang PM, Ollerenshaw JE, Kay LE (2003) Cross-correlated relaxation enhanced 1H[bond]13C NMR spectroscopy of methyl groups in very high molecular weight proteins and protein complexes. *J Am Chem Soc* 125:10420–10428.
45. Rosenzweig R, Kay LE (2014) Bringing dynamic molecular machines into focus by methyl-TROSY NMR. *Annu Rev Biochem* 83:291–315.
46. Tang WK, et al. (2010) A novel ATP-dependent conformation in p97 N-D1 fragment revealed by crystal structures of disease-related mutants. *EMBO J* 29:2217–2229.
47. Tang WK, Xia D (2013) Altered intersubunit communication is the molecular basis for functional defects of pathogenic p97 mutants. *J Biol Chem* 288:36624–36635.
48. Niwa H, et al. (2012) The role of the N-domain in the ATPase activity of the mammalian AAA ATPase p97/VCP. *J Biol Chem* 287:8561–8570.
49. Fernández-Sáiz V, Buchberger A (2010) Imbalances in p97 co-factor interactions in human proteinopathy. *EMBO Rep* 11:479–485.
50. Hänzelmann P, Schindelin H (2011) The structural and functional basis of the p97/valosin-containing protein (VCP)-interacting motif (VIM): Mutually exclusive binding of cofactors to the N-terminal domain of p97. *J Biol Chem* 286:38679–38690.
51. Stach L, Freemont PS (2017) The AAA+ ATPase p97, a cellular multitool. *Biochem J* 474:2953–2976.
52. Rabinovich E, Kerem A, Fröhlich KU, Diamant N, Bar-Nun S (2002) AAA-ATPase p97/Cdc48p, a cytosolic chaperone required for endoplasmic reticulum-associated protein degradation. *Mol Cell Biol* 22:626–634.
53. Cao K, Nakajima R, Meyer HH, Zheng Y (2003) The AAA-ATPase Cdc48/p97 regulates spindle disassembly at the end of mitosis. *Cell* 115:355–367.
54. Kimonis VE, et al. (2000) Clinical and molecular studies in a unique family with autosomal dominant limb-girdle muscular dystrophy and Paget disease of bone. *Genet Med* 2:232–241.
55. Huang R, Pérez F, Kay LE (2017) Probing the cooperativity of *Thermoplasma acidophilum* proteasome core particle gating by NMR spectroscopy. *Proc Natl Acad Sci USA* 114: E9846–E9854.
56. Ripstein ZA, Huang R, Augustyniak R, Kay LE, Rubinstein JL (2017) Structure of a AAA+ unfoldase in the process of unfolding substrate. *eLife* 6:e25754.